

Behavioral Modeling of Dual-band RF PAs using Real-valued Radial Basis Function Neural Networks

Walter B. Pfeffer and Eduardo G. Lima

Grupo de Circuitos Integrados e Sistemas (GICS) - Departamento de Engenharia Elétrica
Universidade Federal do Paraná, Curitiba, Brazil
walterbastospfeffer@gmail.com, elima@eletrica.ufpr.br

Abstract— Behavioral modeling of single-band radio frequency power amplifiers (RFPAs) is commonly performed by real-valued radial basis function neural networks (RVRBFNNs). In behavioral modeling, the RFPA input and output data are complex-valued. Several approaches are available in literature to address the decompositions from complex-to-real and real-to-complex. In this work, the different RVRBFNNs suitable for single-band RFPAs are extended to deal with the behavioral modeling of dual-band RFPAs. Based on a case report, a comparative analysis among 14 different realizations is presented.

Keywords—behavioral modeling; neural network; power amplifier; radio frequency; wireless communications

I. INTRODUCTION

Radio frequency power amplifiers (RFPAs) are widely used in wireless devices [1]-[4]. In this context, the highest possible efficiency is necessary, as the power source for such devices is a battery. An RFPA has its highest efficiency when driven in nonlinear operation regimes. However, to avoid interferences among users of the wireless service, it is not allowed to work with nonlinear devices. Therefore, it is necessary to linearize the RFPA [5] and, for that, a model of its functioning is needed.

In this work, real-valued radial basis function neural networks (RVRBFNNs) are used for setting up such models. RVRBFNNs have within them coefficients which are determined from a supervised nonlinear training algorithm. RVRBFNNs were applied to the modeling of complex-valued input-output data measured on a single-band RFPA in [6]-[9]. The way to represent the input and output values of the RFPA within the RVRBFNN implies in different allegiances of the models, as all values generated by RFPAs are complex-valued and the RVRBFNN involves only real-valued numbers[6]-[9].

In this work, RVRBFNNs are applied to the modeling of complex-valued data from dual-band RFPAs. Thus, the purpose in here is to present and compare several ways to represent and insert these complex-valued input and output values of dual-band RFPAs in one or more RVRBFNNs.

This work is set in 4 sections. After this introductory section, 14 different RVRBFNNs are defined in Section II. Based on a case report, Section III involves the accuracies

achieved by each RVRBFNN realization. Section IV discusses the simulation results and concludes this work.

II. RFPA INPUT AND OUTPUT SIGNAL MODELS

The dual-band RFPA input signal is described as:

$$x_n = |\tilde{x}_n^1| \cos[2\pi f_1 n + \angle \tilde{x}_n^1] + |\tilde{x}_n^2| \cos[2\pi f_2 n + \angle \tilde{x}_n^2] \quad (1)$$

and the output signal is described as:

$$y_n = |\tilde{y}_n^1| \cos[2\pi f_1 n + \angle \tilde{y}_n^1] + |\tilde{y}_n^2| \cos[2\pi f_2 n + \angle \tilde{y}_n^2], \quad (2)$$

where the superscript 1 refers to the first band and the superscript 2 refers to the second band.

To take into account dynamic effects due to non ideal frequency response of RFPA internal circuits [10], the complex-valued instantaneous outputs \tilde{y}_n^1 e \tilde{y}_n^2 must be functions of present and past complex-valued inputs, e.g. functions of \tilde{x}_{n-m}^1 and \tilde{x}_{n-m}^2 for $m = 0, \dots, M$, where M is the RFPA memory length.

To take into account nonlinear effects due to power gain compression of the RFPA [10], the utilization of a RVRBFNN is advised because it employs nonlinear activation functions.

As the terminology indicates, RVRBFNN does not accept complex-valued signals. The complex input envelopes can be represented in polar representation according to:

$$\tilde{x}_n^1 = a_n^1 \exp(j\theta_n^1) \quad (3)$$

and

$$\tilde{x}_n^2 = a_n^2 \exp(j\theta_n^2). \quad (4)$$

The complex output envelopes are first modified by:

$$\tilde{y}_n^1 = \tilde{s}_n^1 \exp(j\theta_n^1) \quad (5)$$

and

$$\tilde{y}_n^2 = \tilde{s}_n^2 \exp(j\theta_n^2). \quad (6)$$

For the case of single-band RFPAs, [6] uses as RVRBFNN

inputs only present and past amplitude components, while [7]-[9] also use the sine and cosine of the difference between two consecutive polar angle components. Again, for the case of single-band RFPAs, [6]-[8] use as RVRBFNN outputs the amplitude and phase components of the modified complex envelope $\tilde{s}_n = |\tilde{s}_n| \exp(j\angle\tilde{s}_n)$, while [9] uses as RVRBFNN outputs the real and imaginary parts of the modified complex envelope $\tilde{s}_n = \text{Re}(\tilde{s}_n) + j \text{Im}(\tilde{s}_n)$. Besides, in [6]-[7] a single RVRBFNN of two outputs is used, while in [8]-[9] two independent RVRBFNNs of single output are used.

Based on the previous studies of [6]-[9] for single-band RFPAs, the general RVRBFNN shown in Fig. 1 can be defined for the modeling of dual-band RFPAs. In Fig. 1, s_n^{1a} , s_n^{1b} , s_n^{2a} and s_n^{2b} refer to the two real-valued components of the modified complex-envelopes, which can be either the real and imaginary parts or the amplitude and phase components.

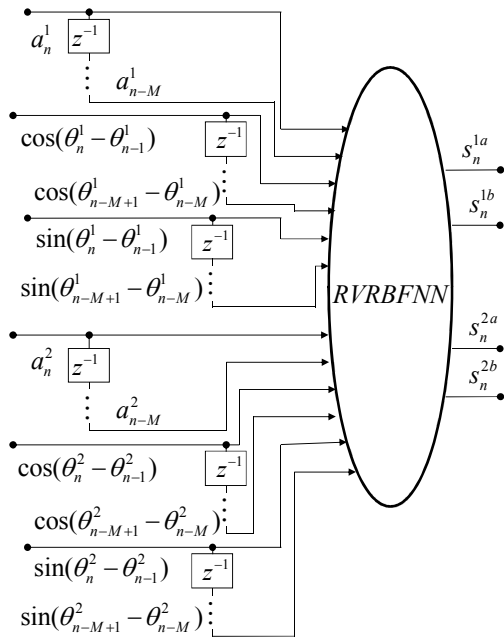


Fig. 1. Block diagram of a general RVRBFNN for dual-band RFPAs.

However, Fig. 1 is not the only possible realization for a RVRBFNN intended for dual-band RFPAs. In fact, as done in [8] and [9], two independent networks can be used. Besides, it is also possible to reduce the number of inputs, as done in [6]. Thereupon, different combinations among many possible cases are created in order to compare and determine the case that presents the best trade-off between modeling complexity and accuracy. To simplify the notation, the following terminology is adopted:

A: a_{n-m}^1 for $m = 0, \dots, M$ are applied as RVRBFNN inputs.

B: a_{n-m}^2 for $m = 0, \dots, M$ are applied as RVRBFNN inputs.

C: $\cos(\theta_{n-m+1}^1 - \theta_{n-m}^1)$ and $\sin(\theta_{n-m+1}^1 - \theta_{n-m}^1)$ for $m = 0, \dots, M$ are applied as RVRBFNN inputs.

D: $\cos(\theta_{n-m+1}^2 - \theta_{n-m}^2)$ and $\sin(\theta_{n-m+1}^2 - \theta_{n-m}^2)$ for $m = 0, \dots, M$ are applied as RVRBFNN inputs.

E: $s_n^{1a} = \text{Re}(\tilde{s}_n^1)$ and $s_n^{1b} = \text{Im}(\tilde{s}_n^1)$ are estimated at the RVRBFNN outputs.

F: $s_n^{2a} = \text{Re}(\tilde{s}_n^2)$ and $s_n^{2b} = \text{Im}(\tilde{s}_n^2)$ are estimated at the RVRBFNN outputs.

G: $s_n^{1a} = |\tilde{s}_n^1|$ and $s_n^{1b} = \angle\tilde{s}_n^1$ are estimated at the RVRBFNN outputs.

H: $s_n^{2a} = |\tilde{s}_n^2|$ and $s_n^{2b} = \angle\tilde{s}_n^2$ are estimated at the RVRBFNN outputs.

Concerning to the use of a single RVRBFNN, the 4 cases reported in Table I are defined in this work.

TABLE I. CASES THAT UTILIZE A SINGLE RVRBFNN

Case	Input	Output
1	AB	EF
2	ABCD	EF
3	AB	GH
4	ABCD	GH

Concerning to the use of two RVRBFNNs, the 10 cases reported in Table II are defined in this work.

TABLE II. CASES THAT UTILIZE TWO RVRBFNNs

Case	Band 1 Input	Band 1 Output	Band 2 Input	Band 2 Output
5	A	E	B	F
6	AB	E	AB	F
7	AC	E	BD	F
8	ABC	E	ABD	F
9	ABCD	E	ABCD	F
10	A	G	B	H
11	AB	G	AB	H
12	AC	G	BD	H
13	ABC	G	ABD	H
14	ABCD	G	ABCD	H

III. CASE REPORT

The 14 distinct realizations of RVRBFNN-based dual-band RFA behavioral models described in Section III are now applied to a case report. The input-output data is collected from a dual-band RFA MATLAB description, composed of a finite impulse response (FIR) filter in series with a polynomial nonlinearity. The RFA stimulus signal is composed of two carrier signals: one carrier at 900 MHz modulated by a 3GPP WCDMA envelope signal and one carrier at 2.5 GHz modulated by an LTE OFDMA envelope signal. The data is sampled at a rate equal to 61.44 MHz.

The network training is performed in MATLAB using a Gauss-Newton nonlinear optimization [11]. All the network parameters (neural network centers, input bias, output bias and weights) are initialized by the value 1. The maximum number of iterations is set to 3000. The memory length M is set to 1. The number of hidden neurons is varied. Only RVRBFNNs having at most 50 parameters are trained.

The modeling accuracy is measured by the normalized mean square error (NMSE) [12], according to:

$$NMSE = 10 \log_{10} \left[\frac{\sum_{n=1}^N (\tilde{y}_n^{a,mea} - \tilde{y}_n^{a,es})^2}{\sum_{n=1}^N (\tilde{y}_n^{a,mea})^2} \right], \quad (7)$$

where N is the total number of samples, the superscript *mea* refers to the complex envelope measured at the RFPA output, the superscript *es* refers to the complex envelope estimated by the RVRBFNN model and the superscript *a* refers to which band is being calculated (1 or 2).

The measured data is divided in one subset for network training and one for evaluating the modeling accuracy. All the reported results are, therefore, obtained using the test set.

In a first scenario, the purpose is to verify if the using of input amplitudes at both bands is required to estimate the complex-valued envelope at a specific band. In other words, the importance of using a_{n-m}^2 for estimating \tilde{y}_n^1 , as well as of using a_{n-m}^1 for estimating \tilde{y}_n^2 , is evaluated. Tables III and IV present the best NMSE results for estimating \tilde{y}_n^1 and \tilde{y}_n^2 , respectively.

TABLE III. NMSE RESULTS OBTAINED USING (AND NOT USING) a_{n-m}^2 AS INPUT FOR ESTIMATING \tilde{y}_n^1

Input a_{n-m}^2	NMSE (dB)
absent	-20.66
present	-29.79

TABLE IV. NMSE RESULTS OBTAINED USING (AND NOT USING) a_{n-m}^1 AS INPUT FOR ESTIMATING \tilde{y}_n^2

Input a_{n-m}^1	NMSE (dB)
absent	-21.09
present	-28.69

In a second scenario, the purpose is to verify the necessity of using phase information on the previous time instant. In other words, the importance of using $\cos(\theta_{n-m+1}^1 - \theta_{n-m}^1)$ and $\sin(\theta_{n-m+1}^1 - \theta_{n-m}^1)$ for estimating \tilde{y}_n^1 , as well as of using

$\cos(\theta_{n-m+1}^2 - \theta_{n-m}^2)$ and $\sin(\theta_{n-m+1}^2 - \theta_{n-m}^2)$ for estimating \tilde{y}_n^2 , is now evaluated. Table V reports the best NMSE results.

TABLE V. NMSE RESULTS OBTAINED USING (AND NOT USING) PAST INPUT PHASE INFORMATION

Past input phase information	NSME (dB) for \tilde{y}_n^1	NSME (dB) for \tilde{y}_n^2
present	-20.66	-21.09
absent	-19.21	-19.76

In a third scenario, the purpose is to determine whether to use a rectangular decomposition or a polar decomposition at the network output. In other words, the cases in which the RVRBFNNs have as outputs $s_n^{1a} = \text{Re}(\tilde{s}_n^1)$, $s_n^{1b} = \text{Im}(\tilde{s}_n^1)$, $s_n^{2a} = \text{Re}(\tilde{s}_n^2)$ and $s_n^{2b} = \text{Im}(\tilde{s}_n^2)$ are compared to the cases in which the RVRBFNNs have as outputs $s_n^{1a} = |\tilde{s}_n^1|$, $s_n^{1b} = \angle \tilde{s}_n^1$, $s_n^{2a} = |\tilde{s}_n^2|$ and $s_n^{2b} = \angle \tilde{s}_n^2$. Table VI reports the best NMSE results.

TABLE VI. NMSE RESULTS OBTAINED USING EITHER THE RECTANGULAR DECOMPOSITION OR THE POLAR DECOMPOSITION AT THE RVRBFNN OUTPUTS

RVRBFNN output decomposition	NSME (dB) for \tilde{y}_n^1	NSME (dB) for \tilde{y}_n^2
rectangular	-27.90	-28.54
polar	-29.79	-28.69

In a fourth scenario, the benefits of using one or two networks are addressed. To that purpose, Fig. 2 shows the best NMSE results as a function of the number of network coefficients.

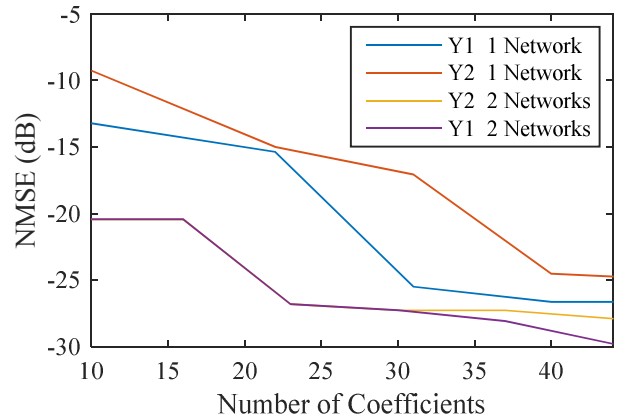


Fig 2. NMSE results when using different number of neural networks.

Finally, Figs. 3 and 4 show the normalized output amplitude as a function of the normalized input amplitude for the two bands. Observe that the best RVRBFNN model is in accordance with the measured input-output data.

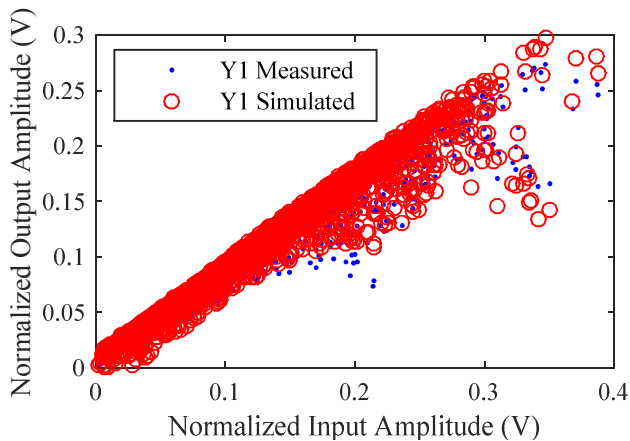


Fig. 3. Measured and best estimated normalized output amplitude as a function of the normalized input amplitude for band 1.

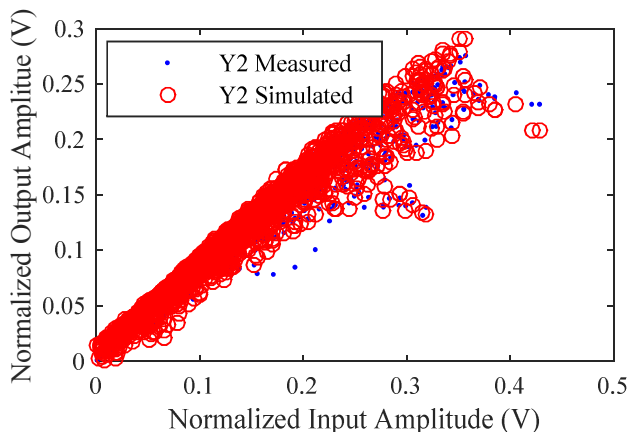


Fig. 4. Measured and best estimated normalized output amplitude as a function of the normalized input amplitude for band 2.

IV. DISCUSSIONS AND CONCLUSIONS

Based on the results reported in Section III, it can be concluded that, for the input-output data used, it is of extreme necessity the use of information on the magnitude of both sets of entries for the creation of an accurate model for the dual-band RFPA.

However, the use of past information about the phase of the input envelope signals provides only negligible improvements in modeling accuracy. Therefore, a better trade-off between computational complexity (e.g. number of network parameters) and modeling accuracy is achieved by not using past input phase information.

Concerning to the output decomposition, both approaches (using either real and imaginary or magnitude and phase) resulted in extremely similar NMSE values. Hence, for the input-output data used in this work it is indifferent the use of one or another representation method.

Finally, by a closer look into Fig. 2, it can be seen that, in a scenario of same computational complexity, the adoption of two neural networks (e.g. one network for estimating each band) provides lower NMSE values in comparison to the case of working with just one network.

Thus, among all the analyzed cases, the best value of NMSE is obtained by using the amplitude information at both inputs in two different neural networks. Each network estimates the output at a particular band and the network outputs can estimate either the rectangular or polar components of a modified RFPA output.

ACKNOWLEDGMENT

The authors would like to acknowledge the financial support provided by Pró-reitoria de Assuntos Estudantis da Universidade Federal do Paraná.

REFERENCES

- [1] F. H. Raab, P. Asbeck, S. Cripps, P. B. Kenington, Z. B. Popovic, N. Potheary, J. F. Sevic, and N. O. Sokal, "Power amplifiers and transmitters for RF and microwave," *IEEE Trans. Microw. Theory Tech.*, vol.50, no.3, pp.814–826, Mar. 2002.
- [2] S. Cripps, *RF Power Amplifiers for Wireless Communications*, 2nd edition. Norwood, MA: Artech House, 2006.
- [3] D. Raychaudhuri and N. B. Mandayam, "Frontiers of Wireless and Mobile Communications," *Proc. IEEE*, vol.100, no.4, pp.824-840, Apr. 2012.
- [4] N. Bhushan, J. Li, D. Malladi, R. Gilmore, D. Brenner, A. Damjanovic, R. Sukhvasi, C. Patel, and S. Geirhofer, "Network densification: the dominant theme for wireless evolution into 5G," *IEEE Commun. Mag.*, vol.52, no.2, pp.82,89, Feb. 2014.
- [5] P. B. Kenington, *High Linearity RF Amplifier Design*. Norwood, MA: Artech House, 2000.
- [6] M. Isaksson, D. Wisell, and D. Ronnow, "Wide-band dynamic modeling of power amplifiers using radial-basis function neural networks," *IEEE Trans. Microw. Theory Tech.*, vol. 53, no. 11, 3422–3428, Nov. 2005.
- [7] E. G. Lima, T. R. Cunha, and J. C. Pedro, "A Physically Meaningful Neural Network Behavioral Model for Wireless Transmitters Exhibiting PM–AM/PM–PM Distortions", *IEEE Trans. Microw. Theory Tech.*, vol. 59, no. 12, pp. 3512–3521, Dec. 2011.
- [8] L. B. C. Freire, C. Franca, and E. G. Lima, "Low-pass equivalent behavioral modeling of RF power amplifiers using two independent real-valued feed-forward neural networks," *Prog. Electromagn. Res. C*, vol. 52, 125–133, 2014.
- [9] L. B. C. Freire, C. Franca, and E. G. Lima, "A Modified Real-Valued Feed-Forward Neural Network Low-Pass Equivalent Behavioral Model for RF Power Amplifiers," *Prog. Electromagn. Res. C*, vol. 57, 43–52, 2015.
- [10] J. C. Pedro and S. A. Maas, "A comparative overview of microwave and wireless power-amplifier behavioral modeling approaches," *IEEE Trans. Microw. Theory Tech.*, vol. 53, no. 4, pp. 1150–1163, Apr. 2005.
- [11] J. Dennis Jr., "Nonlinear least-squares," in *State of the Art in Numerical Analysis: Conference Proceedings*, D. A. H. Jacobs, Ed. London: Academic Press, 1977, pp. 269–312.
- [12] M. S. Muha, C. J. Clark, A. Moulthrop, and C. P. Silva, "Validation of power amplifier nonlinear block models," in *IEEE MTT-S Int. Microwave Symp. Dig.*, Anaheim, Jun. 1999, pp. 759–762.